DOI: 10.19884/j.1672-5220.202405014

Triboelectric Nanogenerators Based on Polyimide Membranes Doped with Barium Titanate Nanoparticles and Multi-Walled Carbon Nanotubes

LIU Jingjing, AFZAL Syed Umer, WANG Kaibo, YAN Jing*
School of Textile Science and Engineering, Tiangong University, Tianjin 300387, China

Abstract: High performance is always the research objective in developing triboelectric nanogenerators (TENGs) for future versatile applications. In this study, flexible triboelectric membranes were prepared based on polyimide (PI) membranes doped with barium titanate (BTO) nanoparticles and multi-walled carbon nanotubes (MWCNTs). The piezoelectric BTO nanoparticles were incorporated to boost the electric outputs by the synergistic effect of piezoelectricity and triboelectricity and MWCNTs were incorporated to provide a microcapacitor structure for enhancing the performance of TENGs. When the mass fraction of the BTO nanoparticle was 10% and the mass fraction of the MWCNT was 0.1%, the corresponding TENG achieved optimum electric outputs (an open-circuit voltage of around 65 V, a short-circuit current of about 20.0 μA and a transferred charge of about 25.0 nC), much higher than those of the TENG with a single PI membrane. The TENG is potentially used to supply energy for commercial light-emitting diodes and as self-powered sensors to monitor human physical training conditions. This research provides a guideline for developing TENGs with high performance, which is crucial for their long-term use.

Keywords: triboelectric nanogenerator (TENG); energy harvesting; multi-walled carbon nanotube (MWCNT); barium titanate (BTO); polyimide (PI)
CLC number: TB332 **Document code**: A
Article ID: 1672-5220(2025)02-0107-09

Open Science Identity (OSID)

0 Introduction

In recent years, wearable electronic devices have completely changed fitness tracking, physical training and entertainment, but due to the limitations of traditional batteries, their energy supply has become the critical issue which needs to be addressed[1]. The triboelectric nanogenerator (TENG) is a contemporary nanopower solution that effectively converts mechanical power into electric power through triboelectricity and electrostatic induction, providing a promising opportunity[2]. The TENG has attracted attention for its versatility in managing various substances and its function as a self-powered sensor, constantly tracking the behavior of external power sources[3-4]. Despite significant progress, there is still room for development in the overall output performance of the TENG to meet numerous utility needs, highlighting the importance of ongoing research and innovation in advancing the TENG technology[5].

Common choices of triboelectric materials for TENGs include polyimide (PI), polytetrafluoroethylene (PTFE) and polydimethylsiloxane (PDMS) due to their electronegativity[6]. PI is favored for TENGs due to its blend durability, chemical resistance, ease of production and ability to withstand wear. By adding particles such as ZnO[7], $SrTiO_3$[8], $ZnSnO_3$[9] and barium titanate (BTO)[10] into polymer materials, the output of the TENG can be enhanced by combining the advantages of piezoelectric and triboelectric effects, and then a specialized layer called a piezoelectric-triboelectric layer is introduced[11]. Among them, BTO nanoparticles have attracted a great interest due to their piezoelectric and dielectric properties, as well as their cost-effectiveness. For example, Yang et al.[12] proposed a TENG enhanced with BTO merging silicone rubber, and the TENG achieved good output performance and flexibility.

Moreover, adding conductive fillers to the triboelectric polymer matrix plays an important role in improving the overall output performance of TENGs by providing a microcapacitor for storing more electrons. In previous researches, various conductive materials, including MXene[13], multi-walled carbon nanotubes (MWCNTs)[14], graphene[15] and silver nanoparticles[16], have been used. Among these materials, MWCNTs stand out not only for their durability and flexibility, but also for their excellent mechanical and thermal properties[17-18]. The microcapacitor, which relies on its high surface area due to its tubular structure and nanoscale dimensions, enables efficient charge trapping and storage, thereby improving the overall output performance of TENGs under specific external pressures[19-20]. In previous studies, BTO nanoparticles are used as the piezoelectric

Received date: 2024-05-23
Foundation item: National Natural Science Foundation of China (No. 52103267)
* Correspondence should be addressed to YAN Jing, email: yanjing@tiangong.edu.cn
Citation: LIU J J, AFZAL S U, WANG K B, et al. Triboelectric nanogenerators based on polyimide membranes doped with barium titanate nanoparticles and multi-walled carbon nanotubes[J]. *Journal of Donghua University (English Edition)*, 2025, 42(2): 107-115.

material to enhance the property, and MWCNTs are used to build the microcapacitor structure within the polymer matrix for performance enhancement.

In this study, a TENG is developed based on nanocomposite membranes of the PI matrix, BTO nanoparticles and MWCNTs (BTO/MWCNT/PI membranes) to combine the piezoelectric effect, microcapacitor effect and triboelectric effect. BTO nanoparticles are incorporated to enhance the combined effects of piezoelectric and triboelectric mechanisms. Furthermore, MWCNTs are used to improve both the current and voltage output through the microcapacitor structure. BTO/MWCNT/PI membranes are prepared by the solution casting method, and their tensile properties, dielectric properties and triboelectric performance are discussed considering BTO and MWCNT mass fractions. High-performance triboelectric materials are expected to be obtained through the study.

1 Materials and Methods

1.1 Materials

BTO nanoparticles with an average diameter of 100 nm were bought from Macklin, China. MWCNTs with a mass fraction of 98%, a diameter of 10–20 nm and a length of around 10–30 μm were bought from Chengdu Organic Chemicals Co., Ltd., China. 4,4′-Oxydianiline (ODA) and 1,2,4,5-pyromelitic dianhydride (PMDA) were purchased from Tianjin Zhongtai Chemical Technology Co., Ltd., China. *N*,*N*-Dimethylformamide (DMF) was purchased from Aladdin, China.

1.2 Preparation of BTO/MWCNT/PI membranes

BTO nanoparticles were subjected to the annealing process at 1 000 ℃ for 10 h to attain the tetragonal crystal structure. The BTO/MWCNT/PI membrane was made by the solution casting method. Firstly, BTO nanoparticles at mass fractions of 5%, 10%, 15% and 20% were added to the ODA/DMF solvent to make a homogenous solution. Secondly, PMDA was added to the solution to get a uniform mixture solution. Thirdly, the mixture solution was scraped onto a clean glass plate to obtain BTO/polyamic acid (PAA) membranes, and then the membranes were put into a muffle oven for thermal imidization at 300 ℃ to obtain BTO/PI membranes (5BTO/PI, 10BTO/PI, 15BTO/PI and 20BTO/PI). Then, BTO/MWCNT/PI membranes were made by adding BTO at a mass fraction of 10% and MWCNTs at mass fractions of 0.1%, 0.2%, 0.3% and 0.4%, which were termed as BTO/0.1MWCNT/PI, BTO/0.2MWCNT/PI, BTO/0.3MWCNT/PI and BTO/0.4MWCNT/PI, respectively. Finally, the nanocomposite membrane was fabricated to get the vertical contact-separation TENG with the working area of 2 cm × 2 cm for testing and characterization.

1.3 Characterization

The structures of BTO/MWCNT/PI membranes were examined by using a field emission scanning electron microscope (Gemini SEM500 ZEISS, Germany). Tensile properties were evaluated by using a universal testing machine (Model 3369, Instron, USA). For dielectric property measurements within the range of $1-1\times10^7$ Hz at room temperature, a high-performance frequency analyzer from NoVo Control Technologies in Germany was utilized. During testing procedures, samples were placed between electrodes (a diameter of 2 cm) to form a microcapacitor structure. An oscilloscope (MDO3014, Tektronix, China) was used to measure the voltage and an electrometer (6517B, Keithley, China) was used to measure the current. The vibrator (JZK10, Sinocera Piezoironics Inc., China) provided pressures at various frequencies.

2 Results and Discussion

2.1 Structure and performance of BTO/PI membranes

As can be seen from Fig. 1(a), the cross-sectional scanning electron microscopy (SEM) image of the PI membrane shows a smooth structure. 5BTO/PI has some increase in the bulges from the cross-sectional view, as shown in Fig. 1(b). For 10BTO/PI, the bulges spread out through the cross-section, as shown in Fig. 1(c). 15BTO/PI and 20BTO/PI exhibit more pronounced agglomerates compared to 10BTO/PI, as shown in Figs. 1(d) and 1(e). The increase of the BTO mass fraction leads to excessive clustering or agglomeration[21].

The stress-strain curves of PI and BTO/PI membranes are shown in Fig. 2. As can be seen, the PI membrane has the strength of about 110 MPa and the fracture strain of nearly 60%. By adding BTO nanoparticles at mass fractions of 5%, 10%, 15% and 20%, the strengths of BTO/PI membranes decrease to the values lower than 80 MPa, and the fracture strains are lower than 30%. This is because the PI chain movement is prohibited by the BTO nanoparticles, and then the BTO/PI membranes are less flexible and prone to break under strains. In addition, excess BTO nanoparticles would cause non-uniform stress distribution in the PI matrix[11].

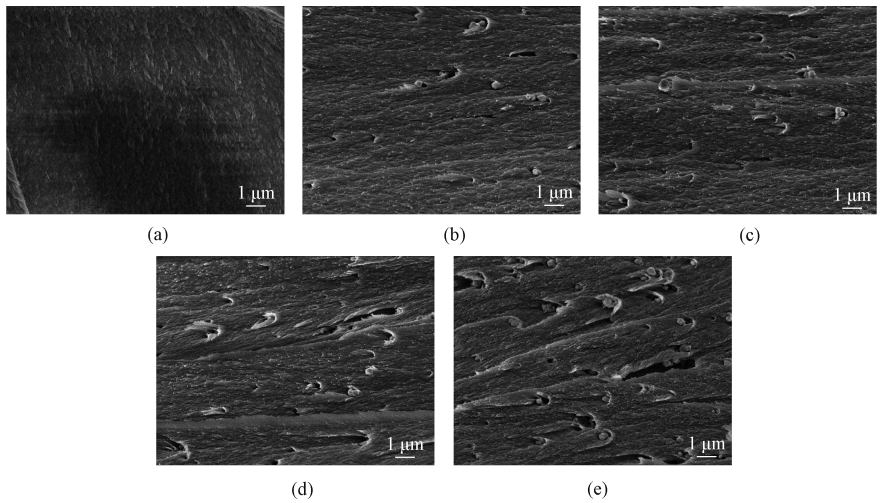

Fig. 1 Cross-sectional SEM images of PI and BTO/PI membranes: (a) PI; (b) 5BTO/PI; (c) 10BTO/PI; (d) 15BTO/PI; (e) 20BTO/PI

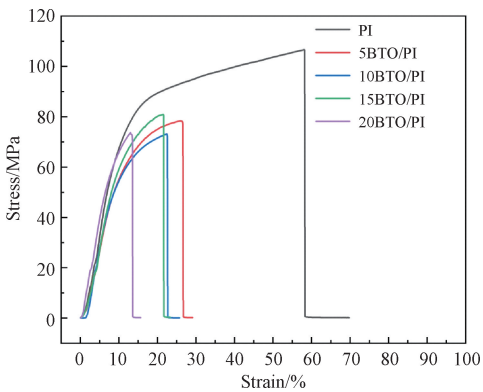

Fig. 2 Tensile properties of PI and BTO/PI membranes

The dielectric properties and conductive properties of PI and BTO/PI membranes are shown in Fig. 3, where δ is the loss angle and tan δ is used to characterize the dielectric loss. The dielectric constant of the PI membrane is 1.5, and that of 20BTO/PI increases to 2.8 due to the high dielectric constant of BTO nanoparticles. Additionally, the presence of BTO nanoparticles may introduce relaxation within the material[22]. This leads to the dielectric loss being about 0.040. As BTO nanoparticles are non-conductive, the conductivity displays non-significant changes by adding BTO nanoparticles.

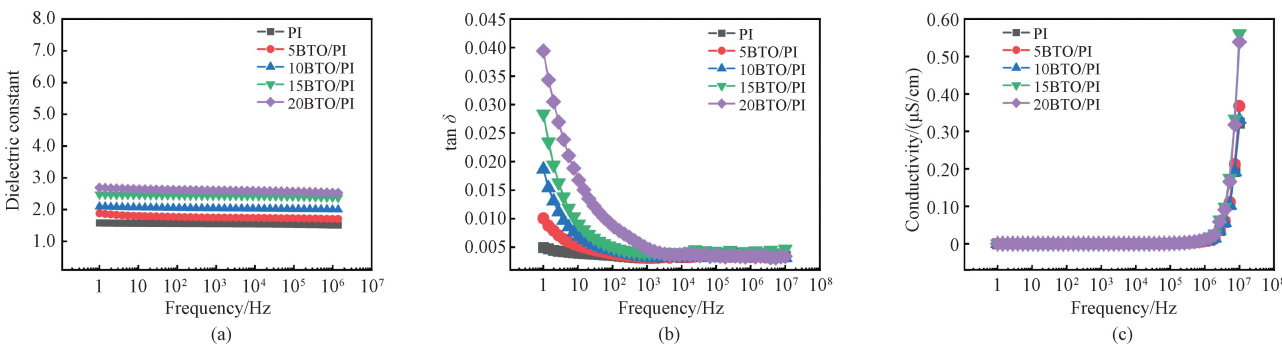

Fig. 3 Dielectric properties and conductive properties of PI and BTO/PI membranes: (a) dielectric constant; (b) dielectric loss; (c) conductivity

To evaluate the effect of BTO mass fractions on the output performance of TENGs, the open-circuit voltage V_{oc}, the short-circuit current I_{sc} and the transferred charge Q_{sc} of TENGs based on BTO/PI membranes at different BTO mass fractions are shown in Fig. 4. There is an initial increase in V_{oc} and I_{sc} as the BTO mass fraction increases. Specifically, at a BTO mass fraction of 10%, V_{oc} and I_{sc} are the highest, being 40 V and 9.9 μA, respectively. It indicates that this mixture offers optimum triboelectric performance. Moreover, the TENG based on 10BTO/PI exhibits the highest Q_{sc} of 14.9 nC. However, a decline in the output performance is observed for the TENG based on BTO/PI membranes at BTO mass fractions higher than 10%, which is attributed to the aggregation of BTO nanoparticles confirmed by their SEM images.

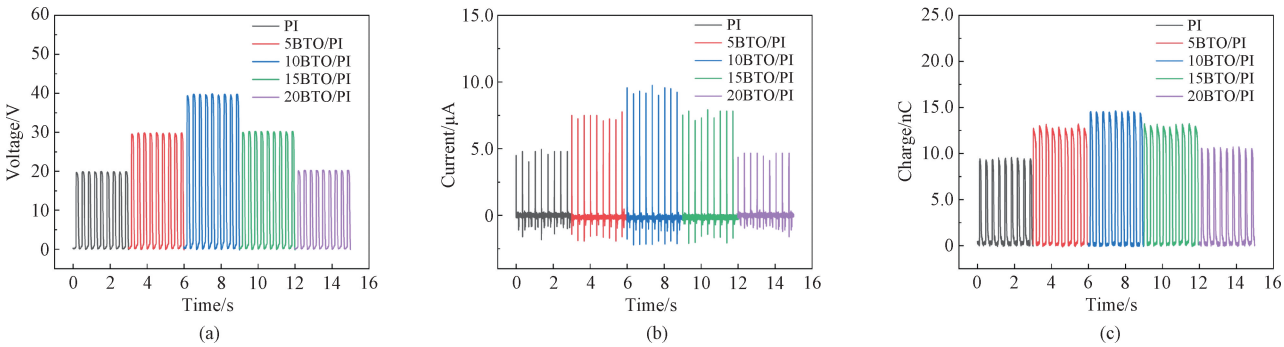

Fig. 4 Output performance of TENGs based on PI and BTO/PI membranes: (a) open-circuit voltage; (b) short-circuit current; (c) transferred charge

2.2 Structure and performance of BTO/MWCNT/PI membranes

For investigating the morphological structure of the membranes, cross-sectional SEM images of BTO/MWCNT/PI membranes were taken. As shown in Fig. 5(a), BTO nanoparticles and MWCNTs are uniformly dispersed in the PI matrix and there is no agglomeration. Figure 5(b) shows the co-existence of BTO nanoparticles and MWCNTs on BTO/0.2 MWCNT/PI. When the MWCNT mass fraction increases to 0.3% and 0.4%, the agglomerates become more prominent in BTO/MWCNT/PI membranes as shown in Figs. 5(c) and 5(d), which is also confirmed in Ref. [23].

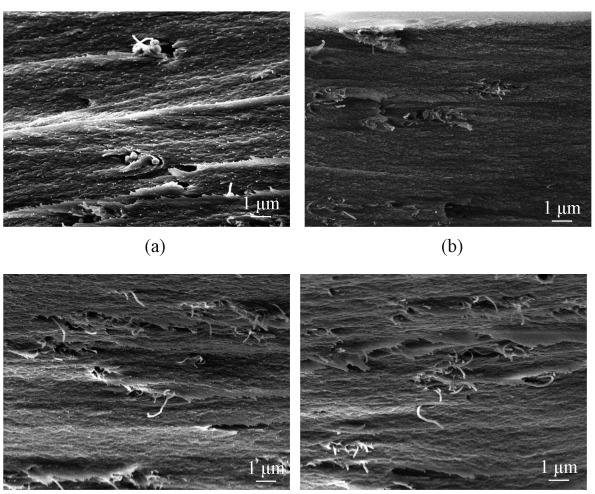

Fig. 5 Cross-sectional SEM images of BTO/MWCNT/PI membranes: (a) BTO/0.1MWCNT/PI; (b) BTO/0.2MWCNT/PI; (c) BTO/0.3MWCNT/PI; (d) BTO/0.4MWCNT/PI

To investigate the tensile properties of the triboelectric layers, the tensile properties of the BTO/MWCNT/PI membranes were tested. The results are shown in Fig. 6. The strength of BTO/0.1 MWCNT/PI is up to 83 MPa, slightly higher than that of 10BTO/PI. The increase in the strength of the BTO/MWCNT/PI membranes by adding MWCNTs can be explained by the fact that MWCNTs are well-known inorganic materials with good tensile properties. However, the strength does not further increase when the MWCNT mass fraction increases. As for the fracture strain, the addition of MWCNTs results in a continuous increase.

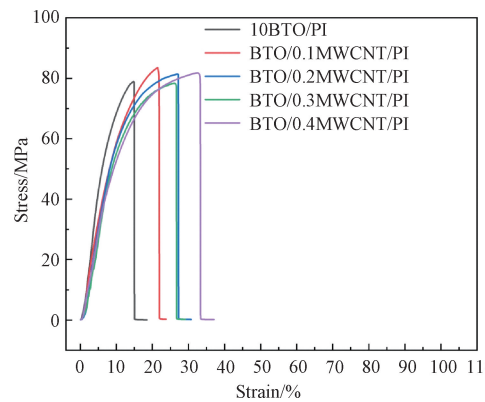

Fig. 6 Tensile properties of 10BTO/PI and BTO/MWCNT/PI membranes

Compared with the PI membrane, BTO/MWCNT/PI membranes have better dielectric properties as shown in Fig. 7. There is a gradual increase in the dielectric constant from 2.0 to 2.7, the dielectric loss from 0.01 to 0.06, and the conductivity from 0.50 μS/cm to 0.75 μS/cm. The reason is that MWCNTs disperse more firmly in the membrane and can form multiple microcapacitors. This network, where MWCNTs act as electrodes with a thin dielectric layer, substantially improves the charge storage capacity. Each microcapacitor provides an exceptionally high capacitance, which can be attributed to the significant increase in the dielectric constant[24]. This suggests that BTO nanoparticle addition further enhances the dielectric properties of the membranes. The dielectric loss of BTO/MWCNT/PI membranes increases with the increase of MWCNT mass fractions because of current leakage caused by the high conductivity of MWCNTs. The presence of MWCNTs improves the conductivity because of their inherent conductive properties.

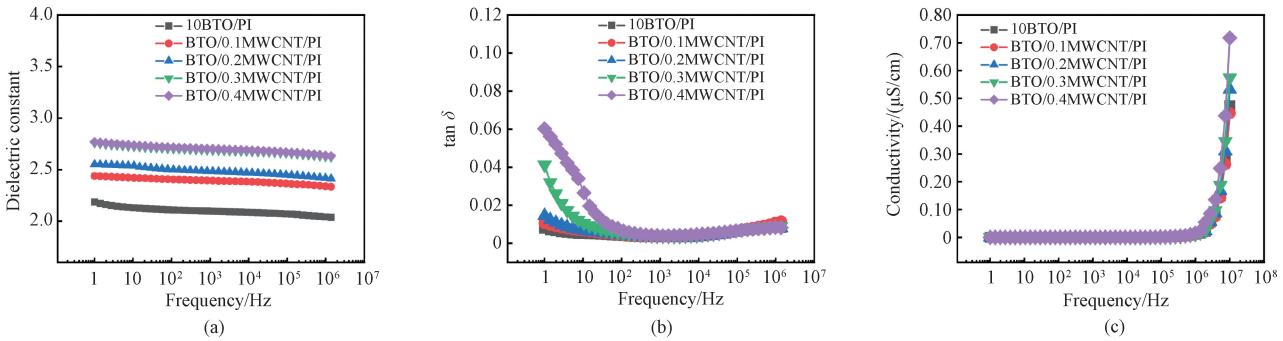

Fig. 7 Dielectric properties and conductive properties of 10BTO/PI and BTO/MWCNT/PI membranes: (a) dielectric constant; (b) dielectric loss; (c) conductivity

Output performance of TENGs based on BTO/MWCNT/PI membranes was tested. The results are shown in Fig. 8. BTO/0.1MWCNT/PI shows the highest open-circuit voltage of around 65 V, short-circuit current of about 20.0 μA and transferred charge of about 25.0 nC because of the synergies between piezoelectric and triboelectric effects as well as the microcapacitor structure formed by MWCNTs[24]. When the mass fraction of MWCNTs further increases, the output performance of the TENG decreases, which may be attributed to the agglomeration of nanofillers or excessive charge loss caused by MWCNTs.

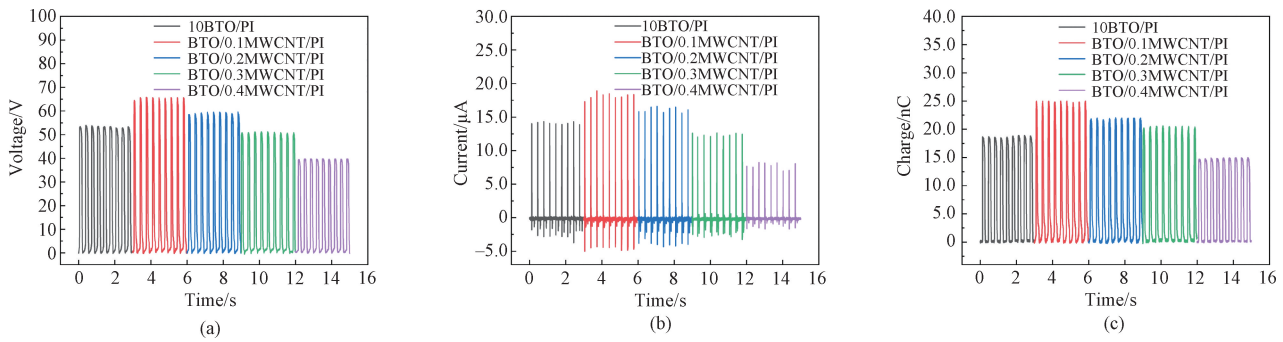

Fig. 8 Output performance of TENGs based on 10BTO/PI and BTO/MWCNT/PI membranes: (a) open-circuit voltage; (b) short-circuit current; (c) transferred charge

2.3 Applications of TENGs based on BTO/MWCNT/PI membranes

To evaluate the output performance of TENGs based on BTO/MWCNT/PI membranes under different conditions, the outputs at different pressures or frequencies were studied. The results are shown in Fig. 9. When the pressure increases from 5 N to 25 N at a frequency of 3.0 Hz, as shown in Figs. 9(a) and 9(b), V_{oc} increases from 18 V to 66 V and I_{sc} increases from 5.0 μA to 18.0 μA. This is because the surface charges on the friction layer are determined by the capacitance and piezoelectric effects. If a higher pressure is applied, the contact between the two friction layers becomes more efficient in helping the generation of charges. When the pressure is 25 N and the frequency varies from 1.0 Hz to 3.0 Hz, V_{oc} presents no significant change because of the unchangeable electrical potential difference, while I_{sc} increases continuously, as shown in Figs. 9(c) and 9(d). Because the increasing frequency accelerates the charge transfer speed, the output current, which depends on the charge transfer speed, increases accordingly.

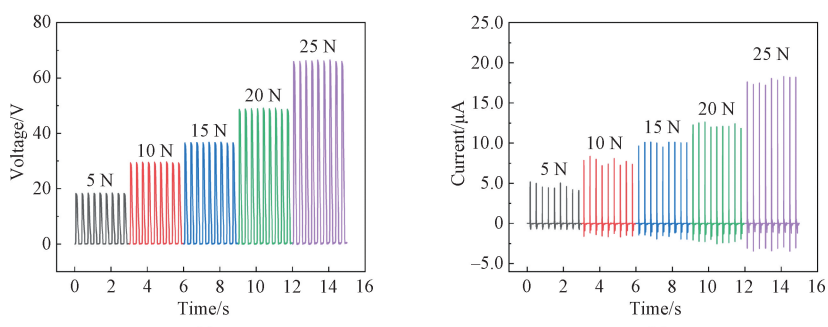

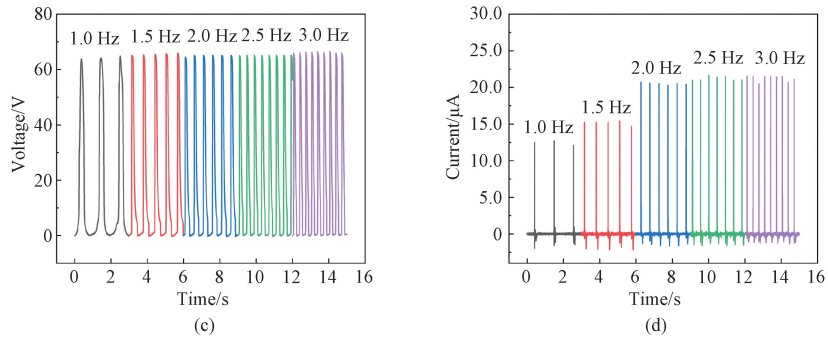

Fig. 9 Output performance of TENGs under different conditions: (a) open-circuit voltage at different pressures; (b) short-circuit current at different pressures; (c) open-circuit voltage at different frequencies; (d) short-circuit current at different frequencies

In order to supply power to microelectronic devices, V_{oc} and I_{sc} of TENGs were measured at a frequency of 3.0 Hz, a pressure of 25 N and an external load resistance R from 1×10^4 Ω to 1×10^{10} Ω. The results are shown in Fig. 10. With the increase of R, V_{oc} increases but I_{sc} decreases.

The power density P of the BTO/MWCNT/PI membrane is calculated based on

$$P = \frac{U^2}{RA},$$

where U is the instantaneous peak voltage; A is the working area.

As R increases, P increases gradually first and then decreases. The peak power density is about 0.5 W/m^2 at R of 1×10^9 Ω[23].

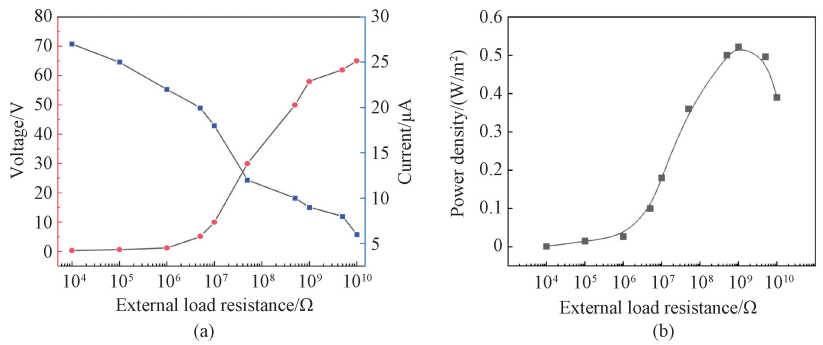

Fig. 10 Output performance of TENGs at different external load resistances: (a) open-circuit voltage and short-circuit current; (b) power density

In order to harness ambient power for sustainable applications, the integration of TENG-based sensors into wearable electronics was studied. The BTO/MWCNT/PI membrane-based TENG can charge different microcapacitors with capacitances of 0.22, 1.00 and 4.70 μF in terms of voltages, as shown in Fig. 11(a). It is indicated that the TENG can be used to store charges which would then be used for lighting up different light-emitting diodes (LEDs) as shown in Fig. 11(b). This novel method allows the seamless integration of TENG-based sensors into diverse wearable devices, such as smartwatches, health trackers and fitness monitors.

Figure 11(c) illustrates the generation of charges through pressure changes on the TENG-based sensor by the movement of feet. The black and red lines represent the output performance of TENGs on the heel and toes in 1.0 s, respectively. TENG-based sensors can detect gestures or commands when the TENG at the foot strikes the ground, generating a detectable current. Similarly, while the pressure is on the toe area, the TENG on the toes would generate signals, and the TENG on the heel would show released pressures. For walking, the speed of the foot movement is low, so the TENG on the toes shows a low current, and the TENG on the heel is landed on the ground and shows a high current. Conversely, for running, the TENG on the toes shows a high current but the TENG on the heel still shows a current higher than that for walking, which shows that the frequency of foot movement increases and implies the state of running. This would be implemented in digital reality applications, or as a hands-unfastened interface for controlling digital devices, and could help in the gesture recognition.

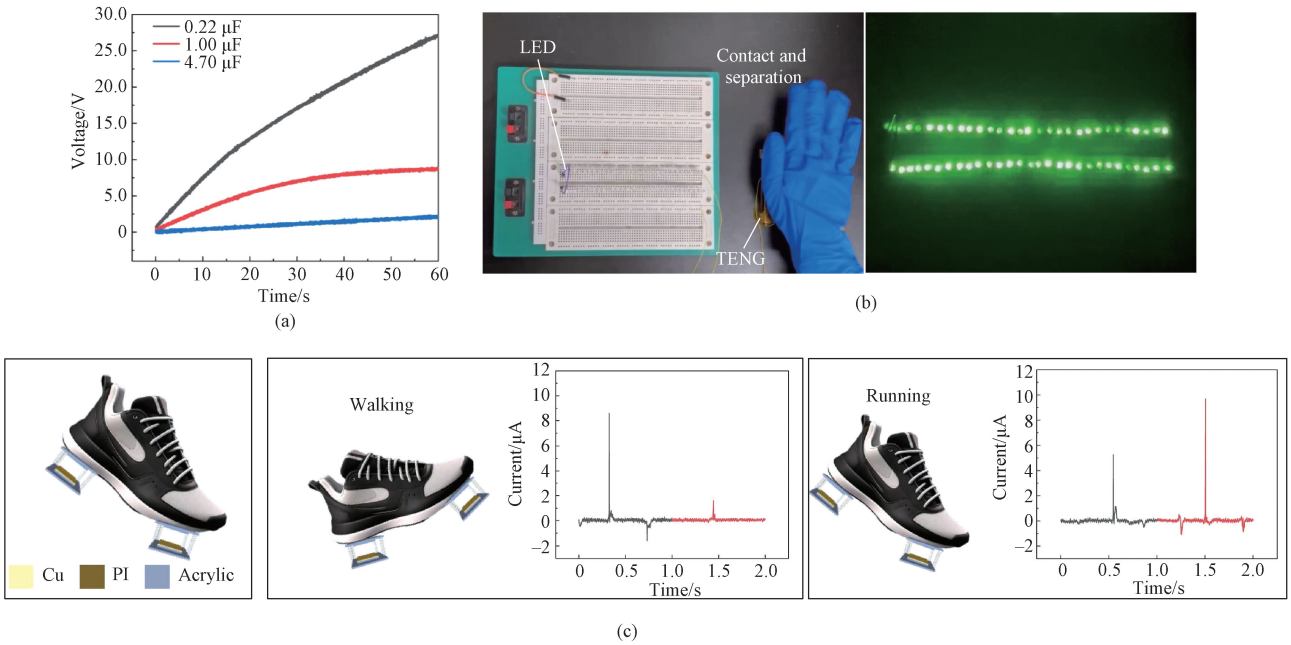

Fig. 11 TENG actual power supply capacity and application: (a) charging process for commercial capacitors; (b) commercial LEDs; (c) motion sensing

3 Conclusions

The integration of flexible PI membranes with BTO nanoparticles and MWCNTs has demonstrated significant advancements in the performance of the TENG. Systematic testing at different compositions determines that a membrane comprising BTO nanoparticles (a mass fraction of 10%) and MWCNTs (a mass fraction of 0.1%) within the PI matrix yields optimal results. The TENG shows remarkable tensile properties with a strength of 83 MPa, and an enhanced electric output (an open-circuit voltage of around 65 V, a short-circuit current of about 20.0 μA and a transferred charge of about 25.0 nC). The high performance of the TENG holds significant promise for a multitude of versatile applications. Specifically, the potential to power commercial LEDs and microelectronics highlights the viability of using TENGs as sustainable energy sources. Additionally, the capacity for self-powered sensors to monitor human physical training conditions signifies a valuable application in wearable fitness technology and can be used for the detection of various body health issues, such as body imbalances, foot misalignment and falls. Such advancements are crucial for ensuring the long-term viability and widespread adoption of the TENG technology across diverse fields, ranging from consumer electronics to healthcare and environmental monitoring.

References

[1] FANG J L, DU J X. Classification of preparation methods and wearability of smart textiles [J]. *Journal of Donghua University (English Edition)*, 2022, 39(4): 379-391.

[2] WU C S, WANG A C, DING W B, et al. Triboelectric nanogenerator: a foundation of the energy for the new era [J]. *Advanced Energy Materials*, 2019, 9(1): 1802906.

[3] XU X, OUYANG Y T, LU S R, et al. Highly flexible and recyclable F-SiO_2/MPU composites for self-powered active motion sensors [J]. *Composites Science and Technology*, 2021, 216: 109068.

[4] YU D M, LIU L F, YU J Y, et al. Enhancing piezoelectric output via constrained phase separation on single nanofibers: harnessing endogenous triboelectricity [J]. *Journal of Donghua University (English Edition)*, 2025, 42(1): 12-19.

[5] MA J, QI X W, ZHAO Y L, et al. Polyimide/mesoporous silica nanocomposites: characterization of mechanical and thermal properties and tribochemistry in dry sliding condition [J]. *Materials & Design*, 2016, 108: 538-550.

[6] LEE J W, YE B U, BAIK J M. Research update: recent progress in the development of effective dielectrics for high-output triboelectric nanogenerator[J]. *APL Materials*, 2017, 5(7): 073802.

[7] SINGH H H, KHARE N. Improved performance of ferroelectric nanocomposite flexible film based triboelectric nanogenerator by controlling surface morphology, polarizability, and hydrophobicity [J]. *Energy*, 2019, 178: 765-771.

[8] CHEN J, GUO H Y, HE X M, et al. Enhancing

performance of triboelectric nanogenerator by filling high dielectric nanoparticles into sponge PDMS film [J]. *ACS Applied Materials & Interfaces*, 2016, 8(1): 736-744.

[9] PARIA S, SI S K, KARAN S K, et al. A strategy to develop highly efficient TENGs through the dielectric constant, internal resistance optimization, and surface modification [J]. *Journal of Materials Chemistry A*, 2019, 7(8): 3979-3991.

[10] ZHANG P, ZHANG W K, DENG L, et al. A triboelectric nanogenerator based on temperature-stable high dielectric $BaTiO_3$-based ceramic powder for energy harvesting[J]. *Nano Energy*, 2021, 87: 106176.

[11] YAN J, LV M D, QIN Y B, et al. Triboelectric nanogenerators based on membranes comprised of polyurethane fibers loaded with ethyl cellulose and barium titanate nanoparticles [J]. *ACS Applied Nano Materials*, 2023, 6(7): 5675-5684.

[12] YANG C J, HE J, GUO Y H, et al. Highly conductive liquid metal electrode based stretchable piezoelectric-enhanced triboelectric nanogenerator for harvesting irregular mechanical energy [J]. *Materials & Design*, 2021, 201: 109508.

[13] SOHEL RANA S M, RAHMAN M T, SALAUDDIN M, et al. Electrospun PVDF-TrFE/MXene nanofiber mat-based triboelectric nanogenerator for smart home appliances [J]. *ACS Applied Materials & Interfaces*, 2021, 13(4): 4955-4967.

[14] LIU Z Q, MUHAMMAD M, CHENG L, et al. Improved output performance of triboelectric nanogenerators based on polydimethylsiloxane composites by the capacitive effect of embedded carbon nanotubes [J]. *Applied Physics Letters*, 2020, 117(14): 143903.

[15] REN C J, BAI Z Q, LIU X J, et al. Preparation and actuated strain properties of functionalized graphene modified polyurethane materials [J]. *Journal of Donghua University (Natural Science)*, 2022, 48(6): 21-28, 35. (in Chinese)

[16] XIA X N, CHEN J, GUO H Y, et al. Embedding variable micro-capacitors in polydimethylsiloxane for enhancing output power of triboelectric nanogenerator [J]. *Nano Research*, 2017, 10(1): 320-330.

[17] YUE L P, ZHANG X Y, LI W D, et al. RETRACTED: a transparent pressure-sensitive adhesive with high electrical conductivity based on water-soluble nano core-shell hollow composite [J]. *Composites Science and Technology*, 2018, 160: 119-126.

[18] SUI J L, DU M Z, JING Y Y, et al. Enhancing accuracy of flexible piezoresistive pressure sensors by suppressing Seebeck effect [J]. *Journal of Donghua University (English Edition)*, 2021, 38(6): 498-503.

[19] KHAN S A, ZHANG H L, XIE Y H, et al. Flexible triboelectric nanogenerator based on carbon nanotubes for self-powered weighing[J]. *Advanced Engineering Materials*, 2017, 19(3): 1600710.

[20] ZHU Y B, YANG B, LIU J Q, et al. A flexible and biocompatible triboelectric nanogenerator with tunable internal resistance for powering wearable devices[J]. *Scientific Reports*, 2016, 6: 22233.

[21] LI Z H, WANG X L, HU Y Q, et al. Triboelectric properties of $BaTiO_3$/polyimide nanocomposite film [J]. *Applied Surface Science*, 2022, 572: 151391.

[22] DOU L Y, LIN Y H, NAN C W. An overview of linear dielectric polymers and their nanocomposites for energy storage [J]. *Molecules*, 2021, 26(20): 6148.

[23] WANG H X, YANG J W, UMER S, et al. Robust multi-walled carbon nanotubes @ thermoplastic polyurethane porous films with conductive fabrics for wearable triboelectric nanogenerators[J]. *Polymer Composites*, 2024, 45(2): 1208-1217.

[24] YAN J, WANG K B, WANG Y Q, et al. Polyimide nanofiber-based triboelectric nanogenerators using piezoelectric carbon nanotube@barium titanate nanoparticles[J]. *ACS Applied Nano Materials*, 2024, 7(11): 13156-13165.

基于钛酸钡纳米颗粒和多壁碳纳米管掺杂聚酰亚胺膜的摩擦纳米发电机

刘晶晶，AFZAL Syed Umer，王凯博，闫　静*
天津工业大学 纺织科学与工程学院，天津 300387

摘　要：开发高性能摩擦纳米发电机（triboelectric nanogenerator，TENG）以满足未来多功能应用需求始终是该领域的研究目标。该文通过掺杂钛酸钡（barium titanate，BTO）纳米颗粒和多壁碳纳米管（multi-walled carbon nanotube，MWCNT）制备聚酰亚胺（polyimide，PI）柔性摩擦电膜：引入压电 BTO 纳米颗粒，通过压电效应和摩擦电效应的协同作用来提高电输出；引入 MWCNT 来构建微电容结构以增强 TENG 的性能。当 BTO 纳米颗粒的质量分数为 10%且 MWCNT 的质量分数为 0.1%时，TENG 可获得约 65 V、20.0 μA 和 25.0 nC 的最佳摩擦电输出性能，远高于纯 PI 膜的 TENG。该 TENG 可为商用发光二级管供电，也可作为自供电传感器来监测人体活动状况。该研究为开发高性能 TENG 奠定了基础，对其长期使用具有重要意义。

关键词：摩擦纳米发电机；能源采集；多壁碳纳米管；钛酸钡；聚酰亚胺